Regression-assisted Classification for CT-based Portal Hypertension Diagnosis

Wuque Cai[1], Jiayi He[1], Xu Guo[2], Hongze Sun[1], Huan Tong[2], Bo Wei[2], Hao Wu[2,*], Dezhong Yao[1,3], and Daqing Guo[1,3,*]

[1] The Clinical Hospital of Chengdu Brain Science Institute, MOE Key Lab for NeuroInformation, China-Cuba Belt and Road Joint Laboratory on Neurotechnology and Brain-Apparatus Communication, School of Life Science and Technology, University of Electronic Science and Technology of China, Chengdu 611731, China
dqguo@uestc.edu.cn

[2] Department of Gastroenterology and Hepatology, West China Hospital, Sichuan University
hxxhwh@163.com

[3] Research Unit of NeuroInformation (2019RU035), Chinese Academy of Medical Sciences, Chengdu 611731, China

Abstract. Portal hypertension (PHT), a critical complication of liver disease, is primarily assessed via invasive procedures that carry inherent risks and discomfort. Recent advancements in deep learning have demonstrated potential for non-invasive diagnostic assistance based on computed tomography (CT) images. However, the small sample size and notable imbalance in PHT clinical data severely restrict the performance of deep learning methods, while the bias introduced by label discretization further compromises model robustness. To address these challenges, we propose a Regression-assisted Classification (RAC) method for non-invasive PHT diagnosis. Firstly, we propose the RAC method instead of direct classification, enabling fine-grained estimation of hepatic venous pressure gradient (HVPG) values before making categorical decisions, thereby reducing the bias caused by discrete label assignment. Moreover, the boundary-aware weighted learning method is proposed to jointly optimize model parameters and the loss function by dynamically assigning online bucket-based weights and enforcing gradient balance across decision boundaries. We show that this approach can significantly reduce the impact of data imbalance and help handle the challenges of small-sample learning in PHT diagnosis. Experiments on our collected clinical CT dataset achieve 83.28% accuracy and 82.69% for the area under the receiver operating characteristic curve in the three-class classification task of PHT, outperforming the cross-entropy baseline by +1.01% and +2.38%, respectively. These results demonstrate leading performance in PHT multi-class classification diagnostic tasks and offer an effective solution for the direct diagnosis of PHT based on CT images.

Keywords: Portal hypertension · Regression-assisted Classification · omputed tomography images · Boundary-aware Weighted learning.

Wuque Cai and Jiayi He contribute equally to this work.

1 Introduction

Portal hypertension (PHT) is a clinical syndrome characterized by abnormally elevated portal pressure, and it is closely linked to the progression of liver disease [2, 13, 21]. The hepatic venous pressure gradient (HVPG) is the gold standard for quantifying PHT severity, with specific thresholds (e.g., >5 mmHg for clinically significant PHT) guiding therapeutic decisions. [1, 24]. However, the current HVPG measurement method is invasive, complicated, and carries risks such as bleeding and infection [2]. As a consequence, there is increasing interest in non-invasive alternatives [12, 15, 19, 22]. Deep learning has recently shown great promise in medical imaging, particularly for non-invasive diagnostic assistance using CT images [7, 10, 18, 23]. These methods can automatically extract key image features, thereby improving diagnostic accuracy and stability while reducing human subjectivity. This makes deep learning a strong candidate for PHT assessment.

Despite its potential, the application of deep learning to CT image-based PHT diagnosis remains underexplored [16]. Existing methods face two main challenges. The first one is the difficulty of modeling continuous HVPG values using pure classification. Most existing deep learning models categorize HVPG into discrete classes, which compromises the continuous nature of HVPG values. This discretization leads to information loss, potentially classifying similar cases into different categories while grouping dissimilar cases together, thereby masking the actual differences between them. The other challenge is data scarcity and heterogeneity. HVPG measurements are difficult to obtain, resulting in a limited amount of labeled data. Many deep learning models rely on large-scale datasets [5, 9, 17], but the scarcity of data makes these models vulnerable to distribution bias. Additionally, clinical HVPG values are unevenly distributed, with a relative scarcity of healthy cases with low values. This imbalance causes models to predict higher HVPG values more frequently, leading to larger errors in predicting lower HVPG values and affecting the overall accuracy of the model. While class imbalance has been studied in medical imaging [3, 6, 26], effective solutions for CT-based PHT staging remain limited.

To address these challenges, we propose a regression-assisted classification (RAC) method. By integrating regression loss into the model, RAC jointly trains classification and regression tasks, preserving the continuous nature of HVPG values and reducing information loss from discrete classification. Additionally, we introduce a novel boundary-aware weighted (BAW) loss to handle small sample sizes and data imbalance. It employs a bucket-splitting strategy to improve data utilization and an adaptive weighting mechanism to prioritize low-frequency targets. Boundary constraints are also incorporated to dynamically regulate loss contributions, thus enhancing the focus of model on low-frequency data and improving generalization. Our main contributions are summarized as follows: (1) We propose a RAC method, unifying classification and regression to mitigate discretization bias by preserving HVPG continuity. (2) We design a BAW loss with adaptive weighting and boundary-aware optimization, improving learning from low-frequency data. (3) Experiments on a clinical CT dataset show our method

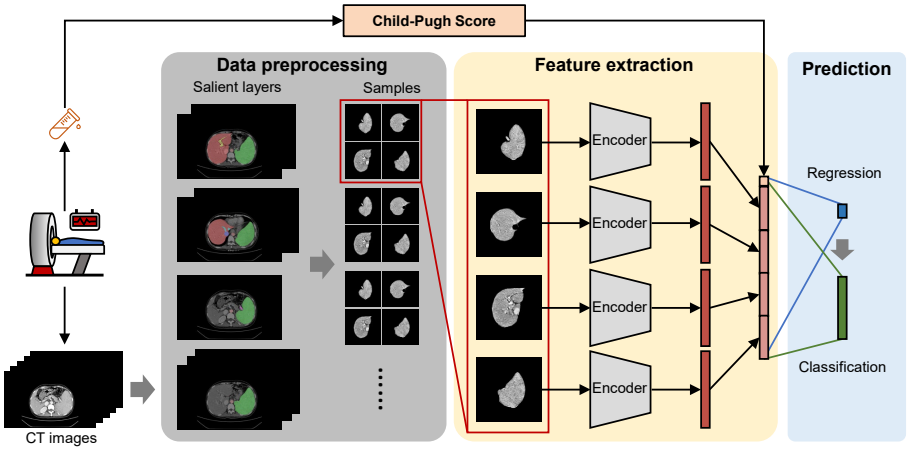

Fig. 1. The overall method of RAC. It consists of data preprocessing module, feature extraction module and prediction module. Child-Pugh score information is combined with CT image processing for assisted prediction.

outperforms existing approaches in PHT classification accuracy, demonstrating strong clinical potential.

2 Method

2.1 Regression-assisted Classification Method

Our proposed RAC method, illustrated in Fig. 1, comprises three main modules: the data preprocessing module, the feature extraction module, and the prediction module. Before the data preprocessing stage, medical professionals first identified salient layers containing key organs and structural tissues from the CT images and delineated regions of interest (ROIs) based on clinical expertise. Notably, different organs and structural tissues may correspond to multiple salient layers (i.e., multiple CT slices).

In the data preprocessing module, we construct a high-quality dataset by ensuring each sample includes salient layers from all key regions. To address data scarcity and standardize sample size, multiple salient layers are aggregated into composite samples, while maintaining strict train-test separation based on medical records to prevent data leakage. In the feature extraction module, spatial and contextual features are extracted from each salient layer using the VPT-Deep [11] model and concatenated with Child-Pugh (CP) scores to integrate imaging and clinical data. The prediction module employs a joint classification and regression head to predict categorical PHT labels and continuous HVPG values. A multi-task loss optimizes both objectives, enhancing diagnostic accuracy and robustness.

2.2 Boundary-aware Weighted Loss for Regression

Currently, there is a lack of regression loss functions specifically designed for imbalanced datasets with limited sample sizes. To address the issue of label imbalance, we draw inspiration from existing work, particularly the Label Distribution-aware Margin (LDAM) [4] method. LDAM is a highly effective approach that introduces adaptive boundaries for different classes based on their sample distribution. By assigning larger boundaries to minority classes and smaller boundaries to majority classes, the LDAM loss forces the model to learn more discriminative feature representations for minority classes. This strategy effectively mitigates the bias of classifier toward majority classes, thereby improving overall performance in imbalanced scenarios. The LDAM loss function is defined as follows:

$$\mathcal{L}_{\mathrm{LDAM}}((x,y);f) = -\log \frac{e^{z_y-\gamma_y}}{e^{z_y-\gamma_y}+\sum_{j\neq y} e^{z_j}}, \tag{1}$$

where $\gamma_j = \frac{C}{n_j^{\frac{1}{4}}}$ represents the decision boundary for a particular class $j \in \{1,\ldots,k\}$, n_j is the number of samples in class j, and $z_y = f(x)_y$ denotes the output of model for input data x and label y. By analyzing the data distribution, the LDAM loss function dynamically adjusts boundary sizes for different classes. This approach limits the influence of the majority class while enhancing the model's focus on learning the minority class.

Inspired by this method and combining it with the scenario of the regression task, we propose a new loss function BAW loss:

$$L_{\mathrm{BAW}} = \frac{1}{N}\left(\sum_{i=1}^{N}\left\{\max\left(0, w_i\cdot\rho_i - M\right)\right\} + \lambda L_1\right), \tag{2}$$

where $\rho_i = \delta^2 \cdot \left(\sqrt{1+\left(\frac{y_i-\hat{y}_i}{\delta}\right)^2}-1\right)$ denotes the Pseudo-Huber loss for a single sample, δ is the hyperparameter, y_i and $\hat{y}_i$ is the true label and predicted value, respectively. Additionally, w_i represents the trainable weight for each sample, M denotes the sample boundary adjustment parameter, and λ is a hyperparameter controlling the regularization strength. The regularization term is formulated as:

$$L_1 = \sum_{j=1}^{B_{in}}\left(w_j \cdot N_j\right), \tag{3}$$

where, B_{in} is the number of sub-buckets, w_j is the weight assigned to the samples in the j-th bucket and N_j is the number of samples in the j-th bucket.

We adopt the Pseudo-Huber function as the baseline loss function, which retains the robustness to outliers and gradient smoothing of the Huber function while addressing its non-differentiability at the critical point. During training, the BAW strategy divides continuous labels into buckets based on the data distribution. Low-frequency data are concentrated in buckets with fewer samples,

enabling better information sharing and reducing the impact of extreme values. The weight w_i is dynamically adjusted to assign higher weights to low-frequency data, mitigating data imbalance. In the optimization process, the model adjusts sample boundaries based on bucket weights. For low-frequency data, the weights increase, leading to wider decision boundaries and larger loss gradients, enhancing their optimization strength. For high-frequency data, the decision boundaries shrink, and loss gradients decrease to prevent over-fitting.

2.3 Learning Method for Regression-assisted Classification

Our proposed RAC method uses gradient descent method to optimize the model. By jointly training the regression and classification tasks, the RAC method is able to learn both continuous values and discrete labels, thus improving the generalization ability and diagnostic accuracy of the model. The overall loss function consists of regression loss and classification loss, and is formally represented as:

$$L_{\mathrm{RAC}} = \frac{1}{2}\left(L_{\mathrm{BAW}} + L_{\mathrm{Classify}}\right), \tag{4}$$

where L_{Classify} is the loss function of classification task. Combining Eq. 2 with the chain derivation rule, we can get:

$$\frac{\partial L_{\mathrm{RAC}}}{\partial \hat{y}_i} = \begin{cases} w_i \cdot \frac{(y_i - \hat{y}_i)}{\sqrt{1+\left(\frac{y_i-\hat{y}_i}{\delta}\right)^2}\cdot\delta} + \frac{\partial L_{\mathrm{Classify}}}{\partial \hat{y}_i}, & \text{if } w_i\left(\rho_i - M\right) > 0 \\ \frac{\partial L_{\mathrm{Classify}}}{\partial \hat{y}_i}, & \text{otherwise} \end{cases}. \tag{5}$$

Meanwhile, the weight gradient of the bucket can be calculated as:

$$\frac{\partial L}{\partial w_i} = \begin{cases} (\rho_i - M) + \lambda \cdot N_j, & \text{if } w_i\left(\rho_i - M\right) > 0 \\ 0, & \text{otherwise} \end{cases}. \tag{6}$$

After gradient back propagation, the parameter θ gradients of the model are:

$$\frac{\partial L}{\partial \theta} = \frac{\partial L_{\mathrm{RAC}}}{\partial \hat{y}} \cdot \prod_{m=k}^{K-1} \frac{\partial \hat{y}}{\partial z^{(m)}} \frac{\partial z^{(m)}}{\partial \theta}, \tag{7}$$

where K is the number of layers.

Based on Eqs. 4-7, we effectively achieve the co-optimization of the loss function and model parameters for the joint regression and classification tasks within the RAC method. This co-optimization enables the model to simultaneously learn continuous and discrete representations, leveraging the complementary information from both tasks to enhance overall performance.

3 Experiments

3.1 Dataset and Metrics

Dataset The clinical dataset, collected from West China Hospital of Sichuan University, includes 285 subjects with CT images annotated at four key anatomical levels (first porta of liver, secondary porta of liver, splenic vein, and spleen) by

Table 1. Comparison with state-of-the-art work.

Dataset	Task	Class	Method	Acc. (%)	F1 (%)	Rec. (%)	Prec. (%)	Spec. (%)	AUC (%)
Liu [16]	C	2	CT-based deep CNN [16]	-	-	92.90	89.00	87.90	91.20
Ours	R	3	LDS [25]	82.19	41.76	42.56	43.18	74.38	-
			FDS [25]	83.73	44.43	47.82	41.89	78.04	-
			LDS+FDS [25]	81.78	40.87	41.95	46.84	74.02	-
			BMC [20]	82.88	46.87	48.88	47.73	76.96	-
			BNI [20]	81.91	40.77	42.24	40.65	73.77	-
			BAW	**84.71**	46.19	47.69	47.65	78.36	-
	C		CE	82.27	50.34	49.92	52.70	78.20	80.31
			Focal [14]	82.03	54.76	53.94	58.10	80.60	76.40
			LDAM [4]	82.59	54.32	52.95	65.68	79.43	81.11
	RAC		CE+**BAW**	83.53	56.69	54.85	64.74	77.74	81.13
			Focal+**BAW**	83.11	50.75	51.24	58.86	78.96	77.16
			LDAM+**BAW**	83.28	**61.55**	**59.58**	**69.59**	**82.39**	**82.69**

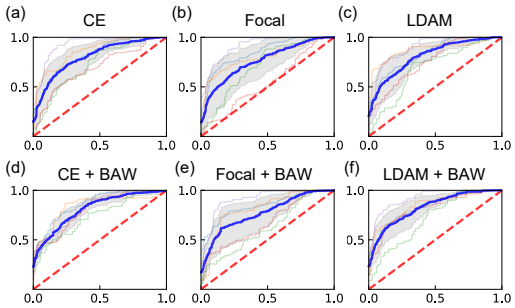

Fig. 2. ROC curves of classification and regression-assisted classification methods.

specialized physicians. Each case contains CP scores and HVPG measurements (2-37mmHg), with a highly imbalanced distribution (HVPG $\leqslant$ 5mmHg : 16 subjects, 5mmHg $<$ HVPG $\leqslant$ 12mmHg : 39 subjects, HVPG $>$ 12mmHg : 230 subjects). We used five-fold cross-validation for robust evaluation.

Metrics To evaluate model performance, we employ accuracy (Acc.), F1 score (F1), recall (Rec.), precision (Prec.), and specificity (Spec.) as evaluation metrics. All metrics, except for accuracy, are computed using the macro-average approach, which calculates the arithmetic mean of the metric values obtained for each class independently. Additionally, we introduce the receiver operating characteristic (ROC) and the area under ROC curve (AUC) to measure the overall discriminative ability across different decision thresholds. This ensures that the evaluation is not dominated by the majority classes and provides a balanced assessment of model performance across all categories.

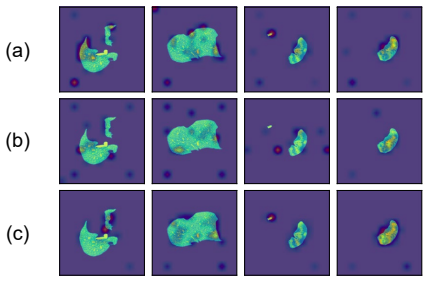

Fig. 3. Visualization results by attention rollout for different tasks. (a)classification, (b)regression and (c)regression-assisted classification.

Table 2. Ablation study for different components in our method on our dataset.

Weighted	Boundary	Acc.(%)	F1(%)	Rec.(%)	Prec.(%)	Spec.(%)
		84.02	45.72	**48.00**	45.85	**78.53**
	✓	83.96	44.23	45.42	**50.36**	75.67
✓		83.51	44.13	44.82	45.23	74.31
✓	✓	**84.71**	**46.19**	47.69	47.65	78.36

3.2 Implementation Details

All experiments were conducted on NVIDIA Tesla A800 GPUs. The encoder is based on the VPT-Deep architecture, with only the parameters of the prompt tokens and the regression head being trained. During preprocessing, we extracted the ROIs from each CT slice, resized the images to 224×224 pixels, and applied luminance normalization and histogram equalization to enhance image quality. For the inconsistent number of CT slices across the four anatomical levels, the slices were reorganized into a total of 1,094 samples. The distribution of these samples based on HVPG values are as follows: 74 samples with HVPG $\leqslant$ 5mmHg, 158 samples with 5mmHg $<$ HVPG $\leqslant$ 12mmHg, and 862 samples with HVPG $>$ 12mmHg. For training, we set the batch size to 32, the learning rate to 0.001, and use the Adam optimizer by default. The training process is run for a total of 50 epochs to ensure convergence. The codes of our fundamental model are available at `https://github.com/GuoLab-UESTC/RAC-for-CT-based-PHT`. The pretrained model weights and data subset for validation can be found at `https://drive.google.com/drive/folders/1DEQ9fm_4E2hIRZOymvecKbUJXfxVcMr4?usp=drive_link`.

3.3 Comparison Study

To validate the RAC method's effectiveness in diagnosing PHT with imbalanced, small-sample data, we conducted comparative experiments. First, we compared the BAW loss with imbalanced regression methods (LDS [25], FDS [25],

BMC [20], BNI [20]). Then, we integrated RAC with imbalanced classification methods (Cross-entropy(CE), Focal Loss [14], LDAM Loss [4]) to test its compatibility. All methods used the same hyperparameters for fairness. Results are shown in Table 1. Notably, R stands for Regression, C stands for Classification, and RAC is our proposed method that have used **BAW** loss.

In regression method comparisons, BAW outperforms BMC in Accuracy (1.83% ↑) and Specificity (1.40% ↑), showing superior overall performance. While slightly lower in recall and precision, BAW achieves a higher correct classification rate and reduces misclassification, demonstrating stable prediction across categories and improved differentiation between majority and minority classes. BAW and other regression methods perform poorly on metrics other than accuracy, indicating a considerable bias in the models. This highlights the need to integrate BAW with classification losses for a more balanced learning process. When combined, CE+BAW improves F1-Score, Recall, and Precision by 6.35%, 4.93%, and 12.04%, respectively, over CE. Compared to Focal Loss, BAW enhances Accuracy, Precision, and AUC. LDAM+BAW outperforms LDAM in all metrics, with F1-Score, Recall, Precision, and Specificity improving by $7.23\%, 6.63\%, 3.91\%$, and 2.96%, respectively. In summary, the RAC method with BAW loss improves classification accuracy and category differentiation, particularly in small-sample imbalanced data scenarios. As shown in Fig. 2, the ROC curves further validate the effectiveness and stability of our proposed RAC method.

3.4 Ablation Study

We first evaluated the loss function without additional mechanisms and found that neither the weighting mechanism nor boundary adjustment alone improves performance. However, their combination significantly enhance model performance, as shown in Table 2. The weighting mechanism adaptively adjusts decision boundaries for different categories, while boundary adjustment ensures stability and prevents bias toward high-frequency categories. Together, they reduce category bias and improve prediction balance under imbalanced data.

We used attention rollout [8] to visualize feature maps for classification-only, regression-only, and RAC models. As shown in Fig. 3, RAC exhibits more focused attention, less noise, and better localization of key regions (e.g., liver edges and texture) compared to the diffuse attention and background noise of other models, further validating the effectiveness in PHT diagnosis.

4 Conclusion

In this study, we propose the RAC method to improve the diagnostic capability for PHT using small-sample, imbalanced CT images. The RAC method integrates regression-assisted classification and a novel BAW loss function, effectively capturing continuous features and enhancing the optimization of low-frequency samples. Experimental results demonstrate that RAC significantly improves the accuracy, robustness, and generalization ability of PHT diagnosis, showcasing its potential for broader medical image analysis tasks.

Acknowledgments. This work was supported by the clinical data provided by West China Hospital of Sichuan University. This work was supported in part by the National Key Research and Development Program of China (grant 2023YFF1204200), in part by the STI 2030–Major Projects (grant 2022ZD0208500), in part by the Sichuan Science and Technology Program (grant 2024NSFTD0032, grant 2024NSFJQ0004 and grant DQ202410).

Disclosure of Interests. The authors have no competing interests to declare that are relevant to the content of this article.

References

1. Berzigotti, A., Seijo, S., Reverter, E., Bosch, J.: Assessing Portal Hypertension in Liver Diseases. Expert review of gastroenterology & hepatology **7**(2), 141–155 (2013)
2. Bosch, J., Abraldes, J.G., Berzigotti, A., García-Pagan, J.C.: The Clinical Use of HVPG Measurements in Chronic Liver Disease. Nature reviews Gastroenterology & hepatology **6**(10), 573–582 (2009)
3. Bria, A., Marrocco, C., Tortorella, F.: Addressing Class Imbalance in Deep Learning for Small Lesion Detection on Medical Images. Computers in biology and medicine **120**, 103735 (2020)
4. Cao, K., Wei, C., Gaidon, A., Arechiga, N., Ma, T.: Learning Imbalanced Datasets with Label-Distribution-Aware Margin Loss. Advances in neural information processing systems **32** (2019)
5. Chen, T., Kornblith, S., Norouzi, M., Hinton, G.: A Simple Framework for Contrastive Learning of Visual Representations. In: International conference on machine learning. pp. 1597–1607. PmLR (2020)
6. Edward, J., Rosli, M.M., Seman, A.: A New Multi-class Rebalancing Framework for Imbalance Medical Data. IEEE Access **11**, 92857–92874 (2023)
7. Gao, X.W., Hui, R., Tian, Z.: Classification of CT Brain Images Based on Deep Learning Networks. Computer methods and programs in biomedicine **138**, 49–56 (2017)
8. Gildenblat, J.: Exploring Explainability for Vision Transformers. `https://jacobgil.github.io/deeplearning/vision-transformer-explainability` (2020)
9. He, K., Zhang, X., Ren, S., Sun, J.: Deep Residual Learning for Image Recognition. In: Proceedings of the IEEE conference on computer vision and pattern recognition. pp. 770–778 (2016)
10. Huang, L., Han, R., Ai, T., Yu, P., Kang, H., Tao, Q., Xia, L.: Serial Quantitative Chest CT Assessment of COVID-19: A Deep Learning Approach. Radiology: Cardiothoracic Imaging **2**(2), e200075 (2020)
11. Jia, M., Tang, L., Chen, B.C., Cardie, C., Belongie, S., Hariharan, B., Lim, S.N.: Visual Prompt Tuning. In: European conference on computer vision. pp. 709–727. Springer (2022)
12. Kim, M.Y., Suk, K.T., Baik, S.K., Kim, H.A., Kim, Y.J., Cha, S.H., Kwak, H.R., Cho, M.Y., Park, H.J., Jeon, H.K., et al.: Hepatic Vein Arrival Time as Assessed by Contrast-enhanced Ultrasonography is Useful for the Assessment of Portal Hypertension in Compensated Cirrhosis. Hepatology **56**(3), 1053–1062 (2012)

13. Kumar, A., Sharma, P., Sarin, S.K., et al.: Hepatic Venous Pressure Gradient Measurement: Time to Learn. Indian J Gastroenterol **27**(2), 74–80 (2008)
14. Lin, T.Y., Goyal, P., Girshick, R., He, K., Dollár, P.: Focal Loss for Dense Object Detection. In: Proceedings of the IEEE international conference on computer vision. pp. 2980–2988 (2017)
15. Liu, F., Ning, Z., Liu, Y., Liu, D., Tian, J., Luo, H., An, W., Huang, Y., Zou, J., Liu, C., et al.: Development and Validation of a Radiomics Signature for Clinically Significant Portal Hypertension in Cirrhosis (CHESS1701): A Prospective Multicenter Study. EBioMedicine **36**, 151–158 (2018)
16. Liu, Y., Ning, Z., Örmeci, N., An, W., Yu, Q., Han, K., Huang, Y., Liu, D., Liu, F., Li, Z., et al.: Deep Convolutional Neural Network-Aided Detection of Portal Hypertension in Patients with Cirrhosis. Clinical Gastroenterology and Hepatology **18**(13), 2998–3007 (2020)
17. Liu, Z., Lin, Y., Cao, Y., Hu, H., Wei, Y., Zhang, Z., Lin, S., Guo, B.: Swin Transformer: Hierarchical Vision Transformer Using Shifted Windows. In: Proceedings of the IEEE/CVF international conference on computer vision. pp. 10012–10022 (2021)
18. Maguluri, L.P., Chouhan, K., Balamurali, R., Rani, R., Hashmi, A., Kiran, A., Rajaram, A.: Adversarial Deep Learning for Improved Abdominal Organ Segmentation in CT Scans. Multimedia Tools and Applications **83**(35), 82107–82129 (2024)
19. Palaniyappan, N., Cox, E., Bradley, C., Scott, R., Austin, A., O'Neill, R., Ramjas, G., Travis, S., White, H., Singh, R., et al.: Non-invasive Assessment of Portal Hypertension Using Quantitative Magnetic Resonance Imaging. Journal of hepatology **65**(6), 1131–1139 (2016)
20. Ren, J., Zhang, M., Yu, C., Liu, Z.: Balanced MSE for Imbalanced Visual Regression. In: Proceedings of the IEEE/CVF Conference on Computer Vision and Pattern Recognition. pp. 7926–7935 (2022)
21. Sanyal, A.J., Bosch, J., Blei, A., Arroyo, V.: Portal Hypertension and Its Complications. Gastroenterology **134**(6), 1715–1728 (2008)
22. Sartoris, R., Rautou, P.E., Elkrief, L., Pollorsi, G., Durand, F., Valla, D., Spahr, L., Terraz, S., Soubrane, O., Cauchy, F., et al.: Quantification of Liver Surface Nodularity at CT: Utility for Detection of Portal Hypertension. Radiology **289**(3), 698–707 (2018)
23. Serte, S., Demirel, H.: Deep Learning for Diagnosis of COVID-19 Using 3D CT Scans. Computers in biology and medicine **132**, 104306 (2021)
24. Wang, C., Huang, Y., Liu, C., Liu, F., Hu, X., Kuang, X., An, W., Liu, C., Liu, Y., Liu, S., et al.: Diagnosis of Clinically Significant Portal Hypertension Using CT-and MRI-based Vascular Model. Radiology **307**(2), e221648 (2023)
25. Yang, Y., Zha, K., Chen, Y., Wang, H., Katabi, D.: Delving into Deep Imbalanced Regression. In: International conference on machine learning. pp. 11842–11851. PMLR (2021)
26. Zhao, P., Liu, X., Yue, Z., Zhao, Q., Liu, X., Deng, Y., Wu, J.: DiGAN Breakthrough: Advancing Diabetic Data Analysis with Innovative GAN-based Imbalance Correction Techniques. Computer Methods and Programs in Biomedicine Update **5**, 100152 (2024)